Synthesis, Crystal Structure, and Electrochemical and Magnetic Study of New Iron (III) Hydroxyl-Phosphates, Isostructural with Lipscombite

Yanning Song, Peter Y. Zavalij, Natasha A. Chernova, and M. Stanley Whittingham*

Department of Chemistry and Institute for Materials Research, State University of New York at Binghamton, Binghamton, New York 13902-6000

Received April 9, 2004. Revised Manuscript Received December 20, 2004

Two novel iron (III) hydroxyl phosphates, of general formula $Fe_{2-y}\square_y(PO_4)(OH)_{3-3y}(H_2O)_{3y-2}$ ($y = {}^2/_3$ or 0.82; $\square$ represents vacancy), have been synthesized by the solvothermal method. The Rietveld refinement of the crystal structure from the X-ray powder diffraction was performed in a tetragonal cell with space group $I4_1/amd$. The structure is isotypic with the mineral caminite $Mg_{1.33}[SO_4(OH)_{0.66}(H_2O)_{0.33}]$ and is closely related to the mixed-valence lipscombite $Fe_{2-y}PO_4(OH)$ ($0 \leq y \leq {}^2/_3$). The interconnection of the chains of face-sharing iron octahedra forms the "rod-packing" structure. In $Fe_{1.18}(PO_4)(OH)_{0.57}(H_2O)_{0.43}$ ($y = 0.82$), about 60% of the chain sites are occupied, whereas about $^2/_3$ of the chain sites are occupied in $Fe_{1.33}(PO_4)(OH)$ ($y = {}^2/_3$). The partial occupancy of the Fe^{3+} sites allows the incorporation of other cations into the structure. When $ZnCl_2$ and $NiCl_2$ were added into the hydrothermal mix, iron was partially substituted by these metal ions, giving $Fe_{4/3-z}M_z\square_{2/3}(PO_4)(OH)_{1-z}(H_2O)_z$ (M = Ni, Zn; $z = 0.28$ and 0.26 for Ni and Zn, respectively), and increasing the cation occupation of the chains to about $^2/_3$. The protons of the hydroxyl groups in these compounds can be replaced by lithium ions with structure retention. Lithium can also be incorporated electrochemically into the lattice, and the disordered compounds are good candidates for the cathode for secondary lithium batteries. The compounds exhibit magnetic phase transitions in the temperature range 60 to 90 K; the transition temperature increases with the number of magnetic ions in the chains.

Introduction

Iron hydroxyl phosphates are well-known minerals and important catalysts. The natural minerals include barbosalite $Fe_3(PO_4)_2(OH)_2$,[1−3] rockbridgeite $Fe_5(PO_4)_3(OH)_5$,[4−5] beraunite $Fe_6(PO_4)_4(OH)_5{\cdot}6H_2O$,[6−7] and whitmoreite $Fe_3(PO_4)_2(OH)_2{\cdot}4H_2O$.[8] The structure of some of the minerals is not well determined yet, such as giniite $Fe_5(PO_4)_4(OH)_2{\cdot}2H_2O$.[9] Some of them have varying compositions with the same structure, such as the synthetic ferric giniite with the composition from $Fe_{4.52}(PO_4)_4(OH)_{1.56}(H_2O)_{2.75}$ to $Fe_5(PO_4)_4(OH)_3\ (H_2O)_{4.6}$.[10] Iron phosphates have been identified as efficient catalysts for the selective dehydrogenation of isobutyric acid (IBA) to methacrylic acid, which can be esterified to produce methyl methacrylate, a very important intermediate in a large number of chemical processes.[11] Since the first patent dealing with the preparation and reaction of an iron phosphate catalyst was published in 1971,[12] many patents and research articles have appeared in the literature; these have been reviewed in ref 11. The iron hydroxyl phosphates were first proposed by Ruszala[13] as catalysts in the production of IBA. Barbosalite and lipscombite were also characterized and tested as catalysts.[14]

Gheith[15] applied the name of lipscombite to a series of compounds of general formula $Fe_{2-y}(PO_4)(OH)$ with tetragonal symmetry. Only the tetragonal compounds with $y < {}^2/_3$ have been studied;[16−19] for example, the structure of $Fe_{1.475}(PO_4)(OH)$ ($y = 0.525$) has $P4_32_12$ symmetry with $a = 7.310$ Å and $c = 13.212$ Å.[16] Schmid-Beurmann[20,21] showed the existence of a restricted tetragonal solid solution of general formula $Fe^{III}_{4/3-z/3}Fe^{II}_z(PO_4)(OH)_{1-z}O_z$ ($0.18 < z < 0.60$). The monoclinic dimorphic variety of the ferric end member of this series ($y = {}^2/_3$), $Fe_{1.33}(PO_4)(OH)$, has been synthesized hydrothermally at 400 °C.[22−23]

* Corresponding author. Tel/fax +1-607-777-4623. E-mail: stanwhit@binghamton.edu.

(1) Lindberg, M. L.; Pecora, M. *Am. Mineral.* **1955**, *40*, 952.
(2) Lindberg, M. L.; Christ, C. L. *Acta Crystallogr.* **1959**, *12*, 695.
(3) Redhammer, G. J.; Tippelt, G.; Roth, G.; Lottermoser, W.; Amthauer, G. *Phys. Chem. Miner.* **2000**, *27*, 419.
(4) Moore, P. B. *Science* **1969**, *164*, 1063.
(5) Moore, P. B. *Am. Mineral.* **1970**, *55*, 135.
(6) Fanfani, L.; Zanazzi, P. F. *Acta Crystallogr.* **1967**, *22*, 173.
(7) Moore, P. B.; Kampf, A. R. *Z. Kristall.* **1992**, *201*, 263.
(8) Moore, P. B.; Kampf, A. R.; Irving, A. J. *Am. Mineral.* **1974**, *59*, 900.
(9) Keller, P. *Neues Jahrb. Miner., Monatsh.* **1980**, 49.
(10) Jambor, J. L.; Dutrizac, J. E. *Neues Jahrb. Miner., Monatsh.* **1988**, *159*, 51.
(11) Millet, J. M. M. *Catal. Rev. Sci. Eng.* **1998**, *40*, 1.
(12) Hsueh-Yan Tsu, K. BP 1,250,749, 1971.
(13) Ruszala, F. U. S. Patent 4,410,727, Ashland Oil Inc., 1983.
(14) Millet, J. M. M.; Rouzies, D.; Vedrine, J. C. *Appl. Catal.* **1995**, *124*, 205.
(15) Gheith, M. A. *Am. Mineral.* **1953**, *38*, 612.
(16) Vencato, I.; Mattievich, E.; Mascarenhas, Y. P. *Am. Miner.* **1989**, *74*, 456.
(17) Matvienko, E. N.; Yakubovich, O. V.; Simonov, M. A.; Belov, N. B. *Zh. Strukt. Khim.* **1981**, *22*, 121.
(18) Vocheten, R.; De Grave, E. *Phys. Chem. Miner.* **1981**, *7*, 197.
(19) Rouzies, D.; Moral, P.; Millet, J. M. M. *J. Phys. Chem.* **1995**, *99*, 12576.
(20) Schmid-Beurmann, P. *J. Solid State Chem.* **2000**, *153*, 237.
(21) Schmid-Beurmann, P. *J. Mater. Chem.* **2001**, *11*, 660.

10.1021/cm049406r CCC: $30.25
Published on Web 02/09/2005

Table 1. DCP-AES Results for Iron Phosphates

compound	Fe/P (Zn,Ni/P)	Li/P	chemical formula[a]
Fe-60%	1.19		$Fe_{1.19}(PO_4)(OH)_{0.57}(H_2O)_{0.43}$
Fe-2/3-T	1.37		$Fe_{1.37}(PO_4)(OH)$
Ni-sub	1.05 (0.28)		$Fe_{1.05}Ni_{0.28}(PO_4)(OH)_{0.72}(H_2O)_{0.28}$
Zn-sub	1.11 (0.27)		$Fe_{1.11}Zn_{0.27}(PO_4)(OH)_{0.73}(H_2O)_{0.27}$
Fe-2/3-T-LiI	1.37	0.50	$Li_{0.50}Fe_{1.37}(PO_4)(OH)_{0.50}O_{0.50}$
Fe-2/3-T-$LiNO_3$	1.36	0.73	$Li_{0.73}Fe_{1.36}(PO_4)(OH)_{0.27}O_{0.73}$
Fe-2/3-T-LiOH	1.36	0.83	$Li_{0.83}Fe_{1.36}(PO_4)(OH)_{0.17}O_{0.83}$
Fe-60%-LiI	1.19	0.55	$Li_{0.55}Fe_{1.19}(PO_4)(OH)_{0.02}(H_2O)_{0.43}O_{0.55}$

[a] The general formula is $Fe_{2-y}\square_y(PO_4)(OH)_{3-3y}(H_2O)_{3y-2}$ ($y = {}^2/_3$ or 0.82) and $Fe_{4/3-z}M_z\square_{2/3}(PO_4)(OH)_{1-z}(H_2O)_z$ (M = Ni, Zn; $z = 0.28$ and 0.26 for Ni and Zn, respectively). The reproducibility of the chemical analysis is around 1%.

We report here the synthesis, crystal structure, and electrochemical and magnetic properties of the tetragonal phase of the ferric end member $Fe_{1.33}(PO_4)(OH)$ ($y = {}^2/_3$), together with a ferric hydroxyl-phosphate phase with still less iron in it, that shows the ability to be substituted with other metals, $Fe_{1.18}(PO_4)(OH)_{0.57}(H_2O)_{0.43}$ (y ca. ${}^4/_5$). Their structures are closely related to each other and to those of caminite, $Mg_{1.33}[SO_4(OH)_{0.66}(H_2O)_{0.33}]$,[24] $Fe_{1.21}PO_4(F,OH,H_2O)$,[25] β-Fe_2PO_4O,[26,27] and lipscombite $Fe_{2-y}PO_4(OH)$.[15] We also report the ion-exchange of some of the hydroxyl protons for lithium.

Experimental Section

Synthesis and Initial Characterization. $Fe_{1.18}(PO_4)(OH)_{0.57}(H_2O)_{0.43}$ (**Fe-60%**) was synthesized by the reaction of 0.01 mol ferric chloride (Fisher), 0.04 mol phosphoric acid (Fisher), and 2 mol water. The initial pH of the solution was adjusted to 4.7 by adding methylamine (Aldrich, 40 wt % in water). The reaction mixture was then sealed into a 125-mL Teflon-lined stainless steel autoclave and heated at 170 °C for 3 days and then cooled slowly to room temperature at 0.25 °C/min. After reaction, the pH of the solution was 4.3. The resulting yellow powder was washed with distilled water and then dried at 65 °C for 15 h. When 0.0025 mol of zinc chloride (J. T. Baker) or nickel (II) chloride (Fisher) was added into the hydrothermal system, green zinc-substituted (**Zn-sub**) and nickel-substituted (**Ni-sub**) compounds were obtained.

When the pH was adjusted by triethylamine (99%, Aldrich) to an initial pH of 5.8 (final pH 4.3), tetragonal $Fe_{1.33}(PO_4)(OH)$ (**Fe-2/3-T**) was formed. The resulting green powder was washed with distilled water and then dried at 65 °C for 15 h. **Fe-2/3-T** was also obtained from reaction mixtures of 0.01 mol $FeCl_3$ and 0.02 mol P_2O_5 (J. T. Baker) in 50 mL of ethanol sealed in 125-mL autoclaves and heated at 180 °C and 165 °C, respectively, for 3 days, but the compound was not phase-pure.

The protons in **Fe-2/3-T** and **Fe-60%** were ion-exchanged topotactically with lithium using three methods at different temperatures. In the first method 0.46 g of **Fe-2/3-T** was added to a solution of 2.2 g of LiI (Aldrich) in acetonitrile (Burdick & Jackson) in a nitrogen glovebox. After 5 days reaction at room temperature the yellow-brown product (**Fe-2/3-T-LiI**) was washed several times with acetonitrile before it was dried in a vacuum. A similar procedure was used with **Fe-60%** giving yellow-brown **Fe-60%-LiI**. In the second method, a solid-state approach was used as in the synthesis of $LiMnAsO_4(OH)$,[28] where the exchange was accomplished using lithium nitrate close to its melting point of 264 °C. About 0.51 g of **Fe-2/3-T** was ground with about 2.1 g of $LiNO_3$, then pressed into pellets, which were then heated in air for 3 days at 215 °C. The yellow product (**Fe-2/3-T-$LiNO_3$**) was washed with dilute hydrochloric acid followed by washing with copious distilled water. In the third approach, lithium hydroxide in methanol was used following the method for the topotactic lithium exchange of $VOHPO_4{\cdot}0.5H_2O$ and $LiVOPO_4{\cdot}0.5H_2O$.[29] A mixture of 0.52 g of **Fe-2/3-T** and 2.0 g of $LiOH{\cdot}H_2O$ (Aldrich) was put into 30 mL of methanol, sealed in a 125-mL Teflon-lined stainless steel autoclave, and heated to 90 °C for 5 days. The green product formed (**Fe-2/3-T-LiOH**) was washed with methanol then ethanol before drying under vacuum.

The products were analyzed by DCP-AES, and the results are shown in Table 1. The phase purity of all the materials was checked by powder X-ray diffraction, obtained on a Scintag XDS2000 $\theta-\theta$ powder diffractometer equipped with a Ge(Li) solid-state detector (CuKα radiation). No other phases were detected, but for the lithiated sample very small broad peaks were observed on some patterns (Figure 1b, pattern 3). Thermal analysis was performed on a Perkin-Elmer TGA. The Fourier transform infrared (FTIR) was performed on a Bruker EQUINOX 55 using KBr pellets. The morphologies of the compounds were studied on a JEOL 8900 SEM. The density of the powders was measured by gas displacement using the ideal gas law.[30]

Magnetic Measurements. The magnetic properties were studied using a Quantum Design MPMS XL SQUID magnetometer. The *dc* susceptibility was measured in a magnetic field of 1000 Oe on cooling the samples from 298 to 2 K. Field-cooled (*FC*) and zero-field-cooled (*ZFC*) curves were measured at 100 Oe over the same temperature range. The magnetization curves were measured in magnetic fields up to 5 T. The temperature dependences of the *ac* susceptibility were studied with the *ac* field amplitude $h = 1$ Oe at frequency $f = 100$ Hz from 2 to 298 k. In studies of the frequency dependences of the *ac* susceptibility, a larger $h = 4$ Oe was used and the frequency was varied from 0.05 to 1000 Hz. Before taking *ac* and *ZFC* data, the remnant field was quenched to less than 3 mOe, the sample was cooled in zero field, and the dependences were measured while heating the sample.

Structure Determination. The XRD patterns indicate that the structures of all these compounds are similar to that of $Mg_{1.33}[SO_4(OH)_{0.66}(H_2O)_{0.33}]$.[25] Therefore, that structure was used as the starting model for the refinement by the Rietveld method using

(22) Ijjaali, M.; Malaman, M.; Gleitzer, C.; Pichavant, M. *Eur. J. Solid State Inorg. Chem.* **1989**, *26*, 73.
(23) Torardi, C. C.; Reiff, W. M.; Takacs, L. *J. Solid State Chem.* **1989**, *82*, 203.
(24) Keefer, K. D.; Hochella, M. F., Jr.; DeJong, B. H. W. S. *Acta Crystallogr.* **1981**, *B37*, 1003.
(25) Loiseau, T.; Lacorre, P.; Calage, Y.; Greneche, J. M.; Ferey, G. *J. Solid State Chem.* **1993**, *105*, 417.
(26) Ech-chahed, B.; Jeannot, F.; Malaman, B.; Gleitzer, C. *J. Solid State Chem.* **1988**, *74*, 47.
(27) Ijjaali, M.; Malaman, M.; Gleitzer, C.; Warner, J. K.; Hriljac, J. A.; Cheetham, A. K. *J. Solid State Chem.* **1990**, *86*, 195.
(28) Aranda, M. A. G.; Attfield, J. P.; Bruque, S. *J. Chem. Soc. Chem. Comm.* **1991**, 604.
(29) Lozano-Calero, D.; Bruque, S.; Aranda, M. A. G.; Martinez-Lara, M.; Moreno, L. *J. Solid State Chem.* **1993**, *103*, 481.
(30) Chern, M. Y.; Mariani, R. D.; Vennos, D. A.; DiSalvo, F. J. *Rev. Sci. Instrum.* **1990**, *61*, 1733.

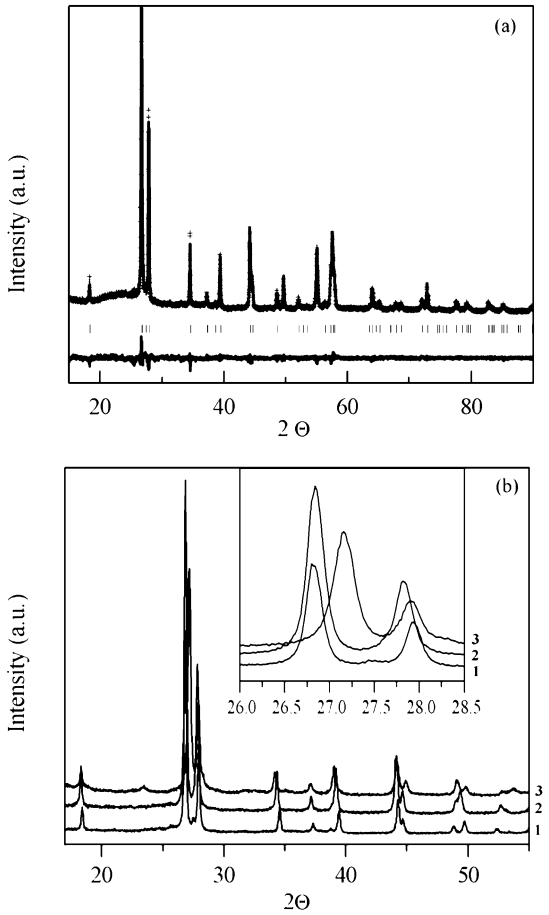

Figure 1. (a) Rietveld refinement plot for **Fe-60%** (observed, +; calculated, solid line; reflections, vertical lines; difference, bottom. (b) XRD patterns of (1) **Fe-2/3-T**; (2) **Fe-2/3-T-LiI**; and (3) **Fe-2/3-T-LiNO$_3$**. The insert shows the change of the pattern at around 27°.

GSAS/EXPGUI system,[31−32] with iron replacing magnesium and phosphorus replacing sulfur. The hydrogen atoms were omitted in the refinement due to their weak electronic density. In the refinement of **Fe-60%** and **Fe-2/3-T**, the cell parameters, atomic positions, isotropic atomic displacement parameters, occupation factors for iron, the scale factor, and profile parameters were varied along with up to 12 background parameters. An absorption correction was also used. The observed and calculated powder patterns for **Fe-60%** are shown in Figure 1a. The experimental X-ray data of **Fe-60%** and **Fe-2/3-T** are summarized in Table 2. The final atomic coordinates, thermal parameters, and occupation factors are presented in Table 3, and selected bond distance and angle data are given in Table 4.

For all the other compounds only the cell dimensions and profile parameters were refined using Materials Studio[33] and GSAS software as reported in Table 5.

Electrochemical Study. For the electrochemical studies, the iron phosphate was mixed with 15 wt % carbon black and 10 wt % PTFE powder; around 20 mg/cm^2 was hot-pressed into a stainless steel Exmet grid for 1 h at about 120 °C. A bag cell configuration was used with a 1 M solution of $LiPF_6$ in 1:1 DMC/EC (EMI, LP30) as the electrolyte, pure lithium as the anode, and Celgard 2400 (Hoechst Celanese Corp.) for the separator. A Macpile galvanostat was used to cycle the cells in a helium-filled glovebox.

(31) Larsen, C. A.; Von Dreele, R. B. *GSAS: General Structure Analysis System*; Los Alamos National Laboratory: Los Alamos, NM, 1990.
(32) Toby, B. *EXPGUI. A Graphical User Interface for GSAS*; NIST Center for Neutron Research: Gaithersburg, MD, 2001.
(33) Accelrys Inc. *Materials Studio*; San Diego, CA, 2001.

Table 2. Crystallographic Data for Fe-60% and Fe-2/3-T

	Fe-60%	Fe-2/3-T
empirical formula	$Fe_{1.18}PO_5$	$Fe_{1.33}PO_5$
Fw	176.55	188.02
crystal system	tetragonal	tetragonal
space group	$I4_1/amd$	$I4_1/amd$
a, Å	5.1803(1)	5.1918(1)
c, Å	13.0341(3)	12.9927(4)
V, Å^3	349.78(1)	350.22(2)
Z	4	4
λ(CuKα), Å	1.54178	1.54178
D_{calc}, g·cm^{-3}	3.353	3.561
D_{meas}, g·cm^{-3}	3.40	3.51
R_{F2}[a]	0.0516	0.0684
R_{prof}[b]	0.0710	0.0983
wR_{prof}[c]	0.0937	0.1299

[a] $R_{F2} = \sum|F_o^2 - F_c^2|/\sum|F_o^2|$. [b] $R_{prof} = \sum|Y_o - Y_c|/\sum Y_o$. [c] $wR_{prof} = [\sum w(Y_o - Y_c)^2/\sum wY_c^2]^{1/2}$.

Table 3. Atomic Coordinates for Fe-60% and Fe-2/3-T

atom	x	y	z	U_{iso}, Å^2	occup.
			Fe-60%		
Fe	0	0.0340(6)	0.4952(4)	0.0147(6)	0.294(1)
P	0	0.75	0.125	0.024(1)	1
O1	0	0.5059(5)	0.1907(2)	0.036(2)	1
O2	0	0.25	0.375	0.013(3)	1
			Fe-2/3-T		
Fe	0	0.0420(5)	0.4939(4)	0.0166(8)	0.3438(9)
P	0	0.75	0.125	0.0134(8)	1
O1	0	0.5045(5)	0.1902(2)	0.026(1)	1
O2	0	0.25	0.375	0.014(2)	1

Table 4. Selected Distances (Å) and Angles (deg) for Fe-60% and Fe-2/3-T

	Fe-60%	**Fe-2/3-T**
P−O1	1.527(2) (4×)	1.531(3) (4×)
Fe−O1 (i,ii)	2.1040(4) (2×)	2.128(3) (2×)
Fe−O1 (iii,iv)	1.9257(1) (2×)	1.909(3) (2×)
Fe−O2 (I)	1.925(5) (1×)	1.885(4) (1×)
Fe−O2 (II)	2.242(4) (1×)	2.280(4) (1×)
Fe−Fe (a)	2.238(7) (1×)	2.160(6) (1×)
Fe−Fe (b,c)	2.5932(5) (2×)	2.6007 (6) (2×)
$O1_{(v,vii)}$-P−$O1_{(vi,viii)}$	108.3(1) (4×)	107.9(1) (4×)
$O1_{(v)}$-P−$O1_{(viii)}$	111.8(2) (1×)	112.8(2) (1×)
$O1_{(vi)}$-P−$O1_{(vii)}$	111.8(2) (1×)	112.8(2) (1×)
$O1_{(i)}$-Fe−$O1_{(ii)}$	87.0(2) (1×)	87.6(2) (1×)
$O1_{(i,ii)}$-Fe−$O1_{(iii)}$	170.6(2) (2×)	168.4(2) (2×)
$O1_{(i,ii)}$-Fe−$O1_{(iv)}$	96.9(1) (2×)	96.9(1) (2×)
$O1_{(iii)}$-Fe−$O1_{(iv)}$	78.1(2) (1×)	76.8(2) (1×)
$O1_{(i,ii)}$-Fe−$O2_{(I)}$	90.9(2) (2×)	97.5(2) (2×)
$O1_{(i,ii)}$-Fe−$O2_{(II)}$	93.1(2) (2×)	92.5(1) (2×)
$O1_{(iii,iv)}$-Fe−$O2_{(I)}$	97.6(2) (2×)	98.0(2) (2×)
$O1_{(iii,iv)}$-Fe−$O2_{(II)}$	78.2(2) (2×)	76.8(2) (2×)
$O2_{(I)}$-Fe−$O2_{(II)}$	174.5(2) (1×)	173.8(2) (1×)

Table 5. Cell Parameters of Iron Phosphates

compound	a(Å)	c(Å)	volume (Å^3)
Ni-sub	5.189(1)	13.016(2)	350.5(2)
Zn-sub	5.1941(3)	13.015(1)	351.1(1)
Fe-2/3-T-LiI	5.2181(1)	12.8942(4)	351.09(2)
Fe-2/3-T-LiNO$_3$	5.2485(2)	12.6405(8)	348.20(4)
Fe-2/3-T-LiOH	5.2493(2)	12.7189(6)	350.47(3)
Fe-60%-LiI	5.2106(1)	12.9135(5)	350.61(2)

Results and Discussion

Synthesis, FTIR, SEM, and Thermal Analysis. The pH of the reaction medium is critical in the synthesis of these iron phosphates. Thus for **Fe-60%**, product with good purity

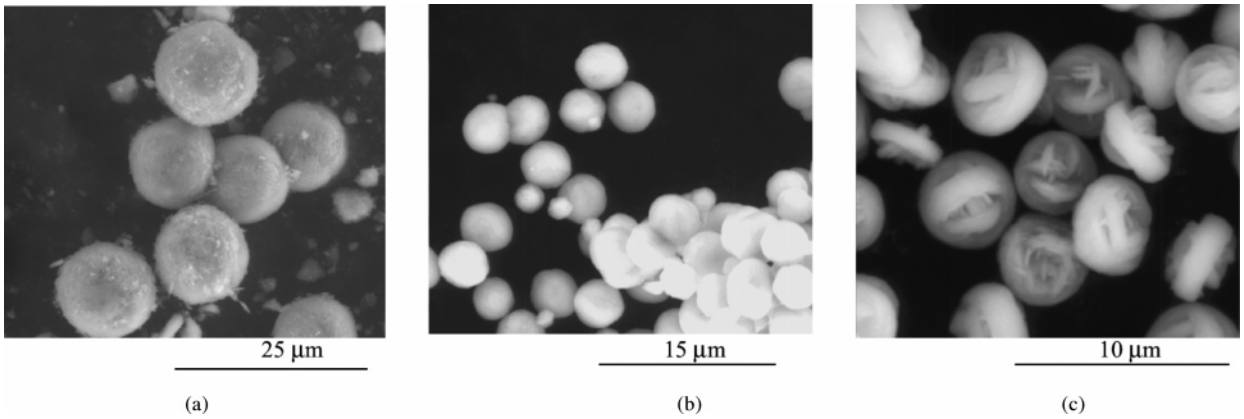

Figure 2. SEM of (a) **Fe-60%**, $Fe_{1.18}(PO_4)(OH)_{0.57}(H_2O)_{0.43}$; (b) **Ni-sub**, $Fe_{1.05}Ni_{0.28}(PO_4)(OH)_{0.72}(H_2O)_{0.28}$; and (c) **Zn-sub**, $Fe_{1.07}Zn_{0.26}(PO_4)(OH)_{0.74}(H_2O)_{0.26}$.

can be obtained only in the pH range of 4.5−4.8. At lower pH, phosphosiderite $FePO_4 \cdot 2H_2O$[34] was obtained; whereas at higher pH, the main product was spheniscidite $Fe_2(NH_4)(OH)(PO_4)_2 \cdot 2H_2O$.[35] Pure phases of the **Ni-sub** and **Zn-sub** compounds were obtained in the pH range of 4.5−5.0. The use of triethylamine as the template results in a pH of 5.8 and yields the **Fe-2/3-T** phase.

The reaction of **Fe-60%** and **Fe-2/3-T** with LiI occurred without the reduction of the iron, as the solution remained colorless even after several days. This is in contrast to the situation for $LiFePO_4$[36] and $FePO_4$[37] where the iron is reduced and iodine is produced. This lack of reduction was confirmed by dissolving the exchanged products, **Fe-60%-LiI** and **Fe-2/3-T-LiI**, in hydrochloric acid followed by addition of $K_4Fe(CN)_6$. No color change to blue was observed showing that all the iron was in the ferric state. Thus, the insertion of lithium into these compounds, as shown in Table 1, is by the ion-exchange of some or all of the protons. The room-temperature exchange resulted in the lowest degree of exchange, 0.50 lithium per phosphorus for LiI, which compares with 0.73 and 0.83 for the elevated temperature reactions with $LiNO_3$ and LiOH. This ion-exchange occurs without major structural changes, but the unit cell expands along the *a* axis and contracts along the *c* axis. The XRD patterns look alike for **Fe-2/3-T**, **Fe-2/3-T-LiI**, and **Fe-2/3-T-LiNO$_3$** as shown in Figure 1b. However, some of the peaks move closer together (e.g., around 27.5° as shown in the insert) or further apart (e.g., around 45°). This reflects the *a* cell parameter increasing and the *c* parameter decreasing on lithium ion-exchange as shown in Table 5. A similar trend was also found in the XRD patterns of **Fe-60%** and **Fe-60%-LiI**.

The IR spectra of all these compounds show the stretching vibration of O−H at ∼3300 cm^{-1} and the P−O stretching vibrations in the region of 1100 cm^{-1} to 900 cm^{-1}. The characteristic vibration of C−N at around 1500 cm^{-1} is absent, indicating that the organic amine is not incorporated into the structure when used as a synthesis template.

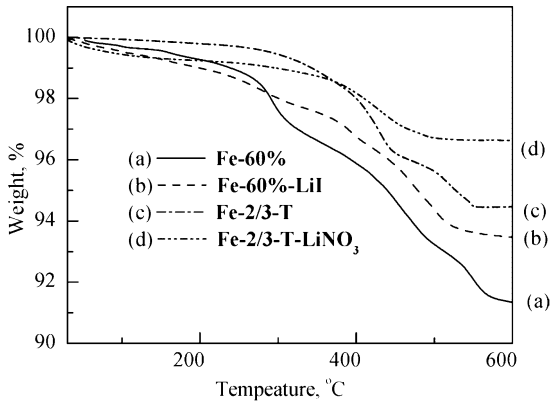

Figure 3. TGA of compounds in oxygen, 5 °C/min. Weight losses below 200 °C are associated with surface adsorbed water.

The morphology of **Fe-60%** and **Ni-sub** is shown in Figure 2 and shows very uniform spherical particles. The average particle sizes are around 10 μm and 4 μm, respectively. However, in the **Zn-sub** compound, the particles look more like donuts with the longest dimension about 3 μm. These particles are all built from tiny plates about a hundred nanometers in size.

The thermal behavior in oxygen atmosphere of **Fe-60%** and **Fe-2/3-T**, as well as their lithiated derivatives, is shown in Figure 3. This behavior gives a measure of the thermal stability, as well as of the proton content; in oxygen the iron remains as ferric. For **Fe-2/3-T** there is almost no weight loss until 300 °C, and the total weight loss is about 5.3%; consistent with the 4.8% expected when the final product contains only Fe^{3+}, O^{2-}, and PO_4^{3-}, for example as in a mixture of $FePO_4$ and Fe_2O_3. The X-ray diffraction pattern of the TGA residue shows several peaks that can be assigned to iron phosphate (ICCD 29-715). The weight loss for **Fe-60%** is higher (8%; calcd. 7.2%), consistent with the presence of lattice water. The weight loss of the lithiated compounds is less than that of the parent compounds due to the lower OH content, 6% (calcd 4.7%) for **Fe-60%-LiI** and 2.5% (calcd 1.4%) for **Fe-2/3-T-LiNO$_3$** consistent with the lower proton content. The X-ray diffraction pattern of the TGA residue from **Fe-60%-LiI** and **Fe-2/3-T-LiNO$_3$** shows

(34) Song, Y.; Zavalij, P. Y.; Suzuki, M.; Whittingham, M. S. *Inorg. Chem.* **2002**, *41*, 5778.
(35) Cavellec, M.; Ferey, G.; Greneche, J. M. *J. Magn. Magn. Mater*. **1997**, *167*, 57.
(36) Yang, S.; Song, Y.; Zavalij, P. Y.; Whittingham, M. S. *Electrochem. Commun.* **2002**, *4*, 239.
(37) Song, Y.; Yang, S.; Zavalij, P. Y.; Whittingham, M. S. *Mater. Res. Bull.* **2002**, *37*, 1249.

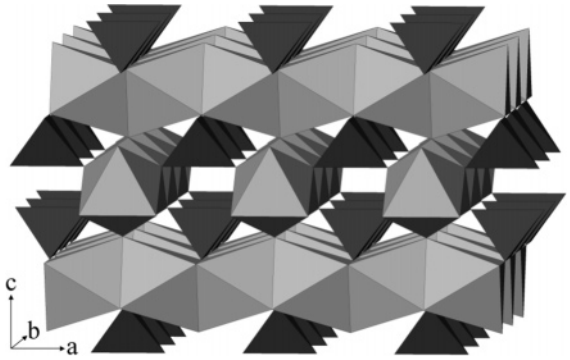

Figure 4. Polyhedral view of compound Fe-60% and Fe-2/3-T showing the "rod-packing" structure.

Li_3PO_4 (ICCD 45-747), $FePO_4$, plus some peaks assignable to $Fe_2O(PO_4)$ (ICCD 45-479).

Structure Descriptions. The structures of **Fe-60%** and **Fe-2/3-T** consist of chains of face-sharing Fe octahedra along [100] and [010] connected by phosphate groups as shown in Figure 4. Phosphate groups interconnect four of these chains to generate a 3D framework. The phosphate tetrahedra are quite regular in both compounds with P−O bond distances of 1.527 Å for **Fe-60%** and 1.531 Å for **Fe-2/3-T** and with O−P−O angles varying from 108° to 113°. The octahedra are slightly distorted with bond distances in the range of 1.93−2.24 Å (av. 2.04 Å) for **Fe-60%**, 1.89−2.28 Å (av. 2.05 Å) for **Fe-2/3-T** and axial angular values in the range of 170.6−174.5° (av. 171.9°) for **Fe-60%**, 168.8−173.8° (av. 170.5) for **Fe-2/3-T**, and the equatorial angular values in the range of 78.1−97.6° (av. 89.9°) for **Fe-60%** and 77.2−98.1° (av. 89.8°) for **Fe-2/3-T**. Tunnels are formed between the chains as shown in Figure 4. Due to the partial occupation of Fe in the chains sites, ions may be able to diffuse from one tunnel to another giving a pseudo 3D diffusion network.

The structures of the above two compounds are closely related to a wide family of structures with general formula $M_y(XO_4)Y_z(H_2O)_{1-z}{\cdot}nH_2O$, including $Mg_{1.33}[SO_4(OH)_{0.66}(H_2O)_{1.33}]$,[24] $Fe_{1.21}PO_4(F,OH,H_2O)$,[25] $VPO_4(H_2O)$,[38] $V_{1.23}[PO_4(OH)_{0.29}(H_2O)_{0.31}]$,[39] $V_{1.28}[PO_4(OH)_{0.84}(H_2O)_{0.16}]{\cdot}0.21H_2O$,[40] and $(V_{0.94}Co_{0.46})[PO_4(OH)_{0.74}(H_2O)_{0.26}]$.[41] In all of these compounds, the transition metal cations occupy $^1/_2$ to $^2/_3$ of the sites in the chain of the face-sharing octahedra.

In these compounds the transition metal occupies the octahedral sites in the chains in a disordered fashion. Thus, in the case of the **Fe-60%** compound, around 58.8% of these sites are occupied, while $^2/_3$ of these sites are occupied in **Fe-2/3-T**. Moreover, it was detected from the difference Fourier maps that the Fe atoms are shifted slightly from the 8d position (0 0 $^1/_2$), due to the repulsion between the two Fe atoms that occupy neighboring octahedra. As a result, in both **Fe-60%** and **Fe-2/3-T,** the Fe−Fe distance increases

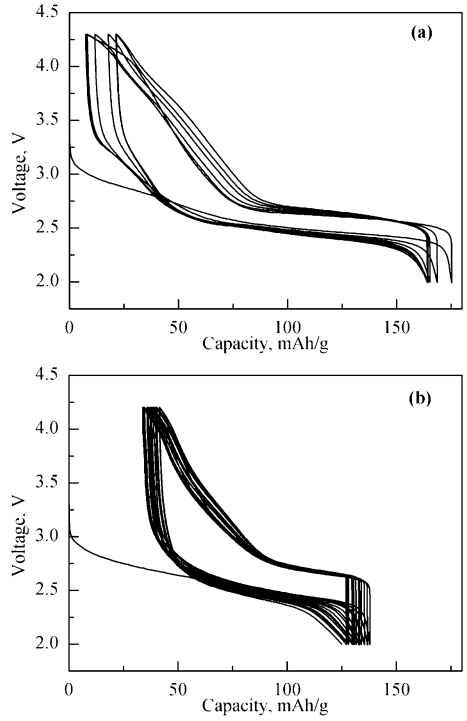

Figure 5. Galvonostatic cycle of Li^+ insertion/extraction using cathode materials of (a) **Fe-2/3-T** and (b) **Fe-60%**. The current density is 0.5 mA/cm^2 (∼15 mA/g). For (a), 192 mAh/g = 1 Li; for (b), 178 mAh/g = 1 Li.

to 2.94 and 3.03 Å, respectively, which is about 0.2 Å greater than the distance between the centers of the FeO_6 octahedra. This is much greater than the Fe−Fe distance, 2.67 Å, found in the compound β-$Fe_2(PO_4)O$[26] where all the octahedral sites are occupied. This is directly related to the much higher site vacancy, about 40% and 33%, respectively, in **Fe-60%** and in **Fe-2/3-T**, which permits the off-center occupancy. This results in less electrostatic repulsion in the chain, giving smaller *a* and *b* cell parameters than in the assumed tetragonal $Fe_2(PO_4)O$ (5.344(5) Å). That is, the more occupied the chain sites, the larger the *a* cell parameter. Thus, the lattice parameter changes from 5.1803(1) Å in **Fe-60%** to 5.1918(1) Å in **Fe-2/3-T**. The higher occupation in **Fe-2/3-T** than **Fe-60%** was also supported by density measurements: 3.51 g/cm^3 for **Fe-2/3-T** and 3.40 g/cm^3 for **Fe-60%** (Table 2).

The ordered occupation of the octahedral sites in **Fe-2/3-T** (two occupied, one empty) yields the dimorphic compound $Fe_4(PO_4)_3(OH)_3$[22] with monoclinic symmetry and an Fe−Fe distance of 2.99 Å. A similar relationship is found between lipscombite (tetragonal) and barbosalite (monoclinic); recently tetrahedral and monoclinic H_2VOPO_4 have also been synthesized.[42]

In the substituted compounds **Zn-sub** and **Ni-sub**, the chain contents are mixtures of iron and zinc or nickel. According to Table 1, the ratio of total metal to phosphorus is roughly 4:3, meaning the chain sites are $^2/_3$ occupied in these compounds as well. Indeed, the cell parameters of **Ni-sub** and **Zn-sub** are quite similar to **Fe-2/3-T** (Table 5). The higher density of **Ni-sub** (3.51 g/cm^3) and **Zn-sub** (3.55

(38) Badraoui, A. E.; Pivan, J. Y.; Maunaye, M.; Pena, O.; Louer, M.; Louer, D. *Ann. Chim. Sci. Mater.* **1998**, *23*, 97.
(39) Vaughey, J. T.; Harrison, W. T. A.; Jacobson, A. J.; Goshorn, D. P.; Johnson, J. W. *Inorg. Chem.* **1994**, *33*, 2481.
(40) Schindler, M.; Joswig, W.; Baur, W. H. *Eur. J. Solid State Inorg. Chem.* **1995**, *32*, 109.
(41) Fur, E. L.; Riou, A.; Pena, O.; Pivan, J. Y. *Solid State Sci.* **2000**, *2*, 135.
(42) Song, Y.; Zavalij, P. Y.; Whittingham, M. S. *J. Electrochem. Soc.* 2005, *152*, accepted for publication.

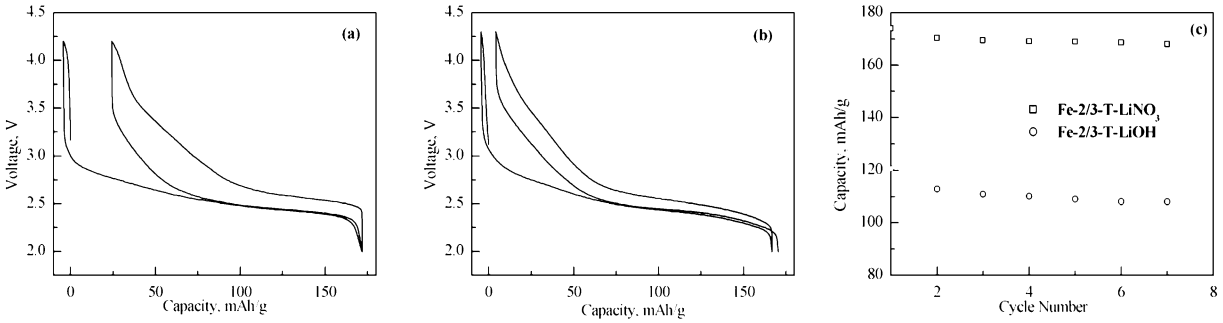

Figure 6. Galvonostatic cycle of Li^+ insertion/extraction using cathode materials of (a) **Fe-60%-LiI**; and (b) **Fe-2/3-T-LiI**. (c) Cycling capacity of **Fe-2/3-T-LiNO$_3$** and **Fe-2/3-T-LiOH**. The current density is 0.2 mA/cm^2 (~5 mA/g).

g/cm^3) than **Fe-60%** (3.40 g/cm^3) also supports that they are more occupied than **Fe-60%**. In another substituted vanadium phosphate compound, $(V_{0.94}Co_{0.46})[PO_4\ (OH)_{0.74}\text{-}(H_2O)_{0.26}]$,[41] the chains contain a mixture of divalent and trivalent cations, V(III) and Co(II).

Due to the partial occupation of the chains, other small cations can be incorporated into the chains. This is probably what happens in the lithium compounds. In **Fe-60%-LiI** and **Fe-2/3-T-LiI**, the chain sites are still not full after lithium incorporation (Table 1). However, in **Fe-2/3-T-LiNO$_3$**, the chain sites are fully occupied by iron and lithium atoms. In **Fe-2/3-T-LiOH**, some of the incorporated lithium atoms might move to the channel sites. This affects the electrochemical behavior as discussed in the next section.

Electrochemical Properties. The electrochemical insertion and removal of lithium at a current density of 0.5 mA/cm^2 is shown in Figure 5. The insertion of lithium was 175 mAh/g for **Fe-2/3-T** and 138 mAh/g for **Fe-60**%; this corresponds to 1.21 and 0.93 Li/P. The reversible capacities are 150 and 100 mAh/g, respectively. At a lower current density of 0.1 mA/cm^2, more than 90% of the lithium insertion is reversible for **Fe-2/3-T** and **Fe-60**%, indicating that lithium diffusion is slow. The theoretical capacities, assuming all the ferric ions can be reduced to ferrous, are 192 and 178 mAh/g for **Fe-2/3-T** and **Fe-60**%, respectively, which are higher than that (169 mAh/g) for $LiFePO_4$ which is currently being extensively studied for use in lithium batteries.[43,44] However, the potential is lower than the 3.5 V of $LiFePO_4$.

The electrochemical behavior of the ion-exchanged **Fe-2/3-T-LiI** is quite similar to the **Fe-2/3-T** before lithium exchange, whereas that of **Fe-60%-LiI** is significantly improved over **Fe-60%**, as shown in Figure 6. No lithium can be removed on an initial charge, indicating that there is no ferrous iron to be oxidized in the ion-exchanged compounds. At the potentials used the Fe(III) cannot be oxidized to Fe(IV), nor would one want to go to Fe(IV) as these ions prefer tetrahedral coordination which would destabilize the lattice. This electrochemical behavior also confirms the earlier conclusion that **Fe-60%** and **Fe-2/3-T** are not reduced when reacted with LiI, the Fe(III)/Fe(II) potential being insufficient to form iodine. The "rod-packing" structure

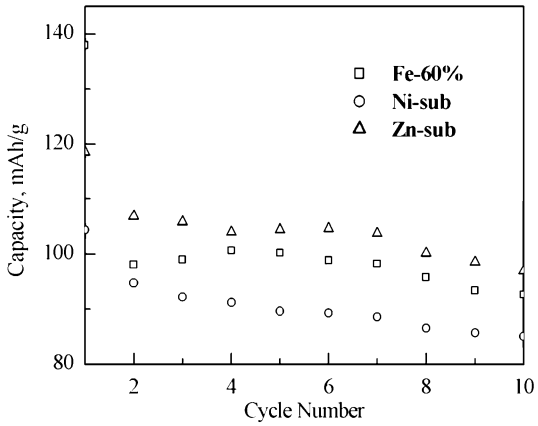

Figure 7. Cycling behavior for **Fe-60%**, **Ni-sub**, and **Zn-sub** at 0.5 mA/cm^2. 170 mAh/g, 149 mAh/g, and 151 mAh/g = 1 Li for **Fe-60%**, **Ni-sub**, and **Zn-sub**, respectively.

stabilizes the channels, into which the lithium ions are believed to be reversibly intercalated; therefore, good cyclability was found in these compounds. As can be noticed in Figure 6c, the electrochemical behavior of the solid-state ionic exchange compound, **Fe-2/3-T-LiNO$_3$**, is much better than the one from solution ion-exchange, **Fe-2/3-T-LiOH**. Possibly, the lithium ions in **Fe-2/3-T-LiNO$_3$** reside in the vacant rod sites, whereas the extra lithium atoms in **Fe-2/3-T-LiOH** (Table 1) move into the channels and hinder the diffusion of lithium during electrochemical cycling. We are working toward clarifying the different lithium environments from ion-exchange and electrochemical intercalation by solid state ^{6}Li NMR.[45]

Although the capacity is lowered after part of the iron is substituted by nickel and zinc, the first cycle capacity loss is dramatically reduced in **Ni-sub** and **Zn-sub**, as shown in Figure 7. After this substitution the chains are more occupied, therefore hindering the lithium from migrating from one tunnel to another and thus any tunnel blockage will be more critical. This is also why the electrochemical behavior of **Fe-2/3-T** is better than **Fe-60%**, as shown in Figure 5.

Magnetic Properties. The temperature dependences of the molar magnetic susceptibilities of these phosphates are plotted in Figure 8a. All the compounds show a rapid increase of susceptibility in the temperature range 50−90 K. At higher temperatures the susceptibility increases slightly

(43) Padhi, A. K., Nanjundaswamy, K. S., Goodenough, J. B. *J. Electrochem. Soc.* **1997**, *144*, 1188.
(44) Whittingham, M. S. *Chem. Rev.* **2004**, *104*, 4271.

(45) Collaboration with C. Grey at SUNY Stonybrook.

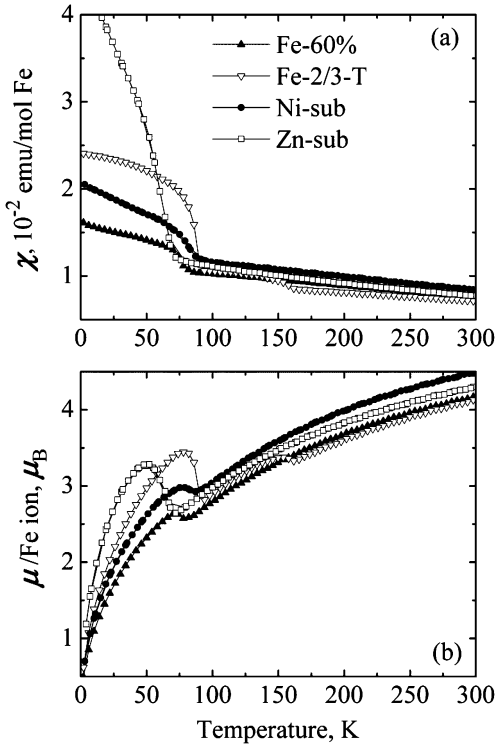

Figure 8. Temperature dependencies of molar magnetic susceptibility measured at 1000 Oe (a) and effective magnetic moment per mole of iron (b) of **Fe-60%**, **Fe-2/3-T**, **Ni-sub**, and **Zn-sub**.

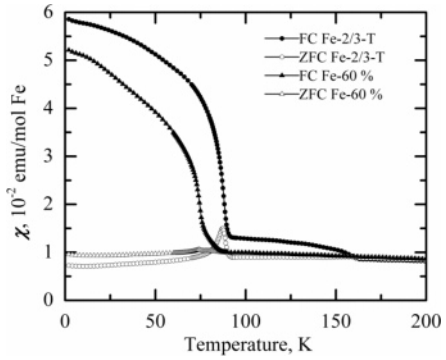

Figure 9. Field-cooled (FC) and zero-field-cooled (ZFC) susceptibilities of **Fe-2/3-T** and **Fe-60%** at 100 Oe.

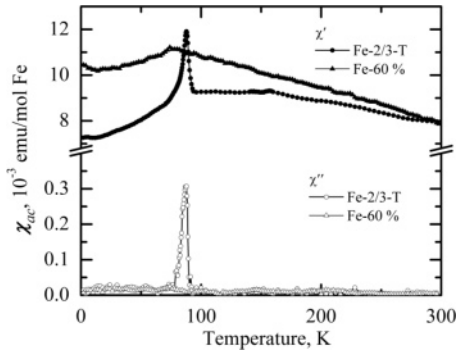

Figure 10. *ac* Susceptibility of **Fe-2/3-T** and **Fe-60%** measured at $f =$ 100 Hz, $h = 1$ Oe.

with temperature decrease in all the compounds except the **Fe-2/3-T**, for which a small steplike transition is observed at about 160 K.

The high-temperature susceptibilities do not follow the Curie−Weiss law. The effective magnetic moment calculated using the paramagnetic relation $\mu = (8\chi_M T)^{1/2}$ is increasing with the temperature [Figure 8b], attaining the values of 4−4.5 μ_B at room temperature. These values are significantly lower than 5.92 μ_B expected for free $S = {}^5/_2$ ion and are close to the values found for monoclinic $Fe_{1.33}(PO_4)(OH)$ from the neutron diffraction data.[43] The observed low values of the effective magnetic moments indicate that the antiferromagnetic alignment of spins found in the monoclinic $Fe_{1.33}(PO_4)(OH)$ might be realized in the tetragonal compounds too and that these antiferromagnetic correlations are partially preserved above the transition temperature.

The magnetization curves measured for **Fe-2/3-T** and **Fe-60%** at 200 K are linear; no hysteresis is observed. The magnetic moments calculated from the slope of these lines agree with the corresponding ones found from the temperature dependences of the susceptibility.

The low-temperature increase of the susceptibility indicates a magnetic phase transition with possible formation of a small net magnetic moment. This is also confirmed by a hysteresis of magnetization found for the above compounds at 10 K. The hysteresis loop observed for **Fe-2/3-T** is characterized by the remnant magnetization $M_r \approx 8.9$ emu/mol Fe and coercive field $H_c \approx 1000$ Oe; for **Fe-60%**, $M_r \approx 2.4$ emu/mol Fe and $H_c \approx 200$ Oe.

The highest transition temperature of 88 K (measured as minimum at $d\chi/dT$ curve) is found in **Fe-2/3-T**. **Ni-sub** orders at 82 K, followed by **Fe-60%** and **Zn-sub,** which have ordering temperatures of 75 and 62 K, respectively. Apparently, the transition temperature increases with the occupation of the chains with magnetic ions.

To learn more about the nature of the magnetic transitions observed we have studied *FC* and *ZFC* curves (Figure 9) and *ac* susceptibilities (Figure 10) of **Fe-2/3-T** and **Fe-60%**. *FC* and *ZFC* curves diverge below 159 and 86 K for **Fe-2/3-T** and **Fe-60%**, respectively. Below 86 K, the deviation, which is the measure of magnetic irreversibility, increases for **Fe-2/3-T**. *ZFC* curve of **Fe-2/3-T** shows a pronounced peak at 87 K and no features at around 160 K, while *ZFC* of **Fe-60%** reveals a very small and wide peak at about 74 K. The *ac* susceptibility data for **Fe-2/3-T** show well resolved peaks at 87 K for both dispersion χ' and absorption χ'', and no peaks at about 160 K, while **Fe-60%** shows a wide peak centered at about 74 K on the dispersion curve and no absorption at all, $\chi'' = 0$ with the accuracy of the experiment.

Thus, the low-temperature magnetic phases in both compounds are irreversible, which can be explained by the blocking of cluster magnetic moments at the transition temperatures. The blocking transition in **Fe-60%** is smeared over a wide temperature range, which can be related to the lower chain occupation. In this case larger variety of the cluster sizes can be achieved, leading to a wide range of blocking temperatures. This also helps to explain the absence of the absorption in the *ac* susceptibility, simply by the fact that at each given temperature the absorption is too small to be detected. The ${}^2/_3$ chain occupation in **Fe-2/3-T** allows ordering of Fe^{3+} ions in pairs separated by the empty site. Therefore, the pairs are expected to be the dominating clusters in this case. However, the Rietveld refinement has

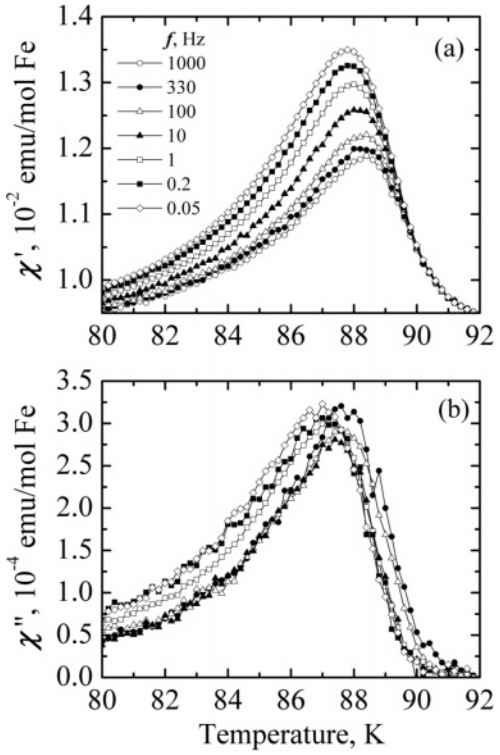

Figure 11. Real (a) and imaginary (b) components of *ac* susceptibility of **Fe-2/3-T** measured at different frequencies and $h = 4$ Oe. The data for χ'' at 1000 Hz are very noisy and are not presented in the figure.

shown that the occupation is slightly higher than $^2/_3$, about 69%, so some triplets and longer clusters should be present in this compound. One would also expect some of these to be present due to the lack of complete ordering of the vacancies. It is interesting to note that the $^2/_3$ occupied ordered compound has the magnetic transition at about 87 K,[23,46] while the $^3/_4$ occupied compound, barbosalite Fe^{2+}-$Fe^{3+}{}_2(PO_4)_2(OH)_2$, in which triplets Fe^{3+}-Fe^{2+}-Fe^{3+} separated by vacancies are present in the chains, orders at 160 K.[3] Therefore, we assume that the small increase of susceptibility found in **Fe-2/3-T** at 160 K reflects the ordering of the small amount of triplets, while the overall formation and blocking of cluster magnetic moments occurs at 88 K.

We have studied temperature dependences of the *ac* susceptibility of **Fe-2/3-T** at various frequencies (Figure 11) to confirm the hypothesis of the blocking transition. We have found that the amplitude of the dispersion peak increases with decreasing *ac* frequency and the peak shifts toward lower temperature (Figure 11a). The same trends are observed in the absorption curves (Figure 11b), though the latter are quite noisy especially at high frequencies and will not be further analyzed. The relative freezing temperature shift $\Delta T_f/T_f$ per decade of frequency $\Delta T_f/[T_f\Delta(\log_{10}\omega)]$ ($\omega = 2\pi f$ is angular frequency) is 0.001, which is somewhat lower than the values of 0.005 to 0.01 typical for canonical spin-glasses,[47] but larger than that in ferro- and antiferromagnets. The latter are usually not observed at low frequencies. It should be noted that the observed shift of 0.5 K over the frequency range studied is readily detected and is comparable to that observed in spin-glasses. However, the freezing temperature of **Fe-2/3-T** is unusually high, which results in small relative shift.

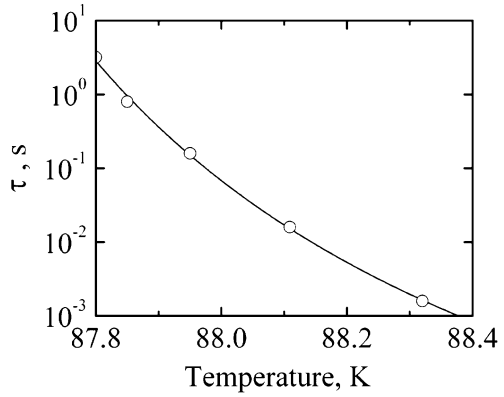

Figure 12. Temperature dependence of the relaxation time calculated from the frequency shift of $\chi'(T)$ maximum over frequency range 0.05−100 Hz and its fit to the Vogel−Fulcher law.

We have further investigated the observed frequency shift by determining and analyzing the temperature dependence of the spin relaxation time τ. We have estimated τ under an assumption that the peaks of $\chi'(T)$ occur at $\omega\tau = 1$. The obtained dependence is shown in Figure 12. Unfortunately, the maxima of the high-frequency peaks are not well defined and the relaxation times found from 330−1000 Hz curves fall out of the monotonic dependence found at lower frequencies. So only the points obtained from 0.05 to 100 Hz $\chi'(T)$ curves are presented in Figure 12.

The best fit to the obtained $\tau(T)$ dependence (solid line in Figure 12) was achieved using the Vogel−Fulcher law appropriate for the system of magnetically interacting clusters, $\tau = \tau_0\exp[E_a/k(T - T_0)]$, where τ_0 is the characteristic relaxation time, E_a is the thermal activation energy, and T_0 is a parameter, which for real glasses is called "ideal glass" temperature.[44] It produces the following parameters: $\tau_0 = 7(3) \times 10^{-9}$ sec, $E_a/k = 17(5)$ K, and $T_0 = 86.9(2)$ K. These values agree well with the typical values characterizing blocking processes. Therefore, we can conclude the magnetic phase transition observed in **Fe-2/3-T** is described by the formation and blocking of cluster magnetic moments.

Concluding Remarks

Several ferric phosphate hydroxides with structures similar to caminite and lipscombite were synthesized and characterized. The chains, made from face sharing of FeO_6 octahedra, are 60% to $^2/_3$ occupied by iron or a mixture of iron and nickel or zinc, and are interconnected to form a "rod-packing" structure. The $^2/_3$ occupied compounds can be ordered or disordered, giving dimorphic compounds with monoclinic and tetragonal symmetry. Some of the protons in these compounds can be replaced by lithium ions. A reversible capacity of more than 170 mAh/g for the tetragonal $^2/_3$ occupied compound makes it a very good candidate for the cathode of a lithium battery. For all the compounds, magnetic phase transitions are observed, the temperatures of which increase from 62 to 88 K as the occupation of the chains with magnetic ions increases.

(46) Malaman, B.; Ijjaali, M.; Venturini, G.; Gleitzer, C.; Soubeyroux, J. L. *Europ. J. Solid State Inorg. Chem.* **1991**, *28*, 519.
(47) Mydosh, J. A. *Spin Glasses: An Experimental Introduction*; Taylor & Francis: London, 1993.

Acknowledgment. We thank Professor Richard Naslund for the DCP-AES analysis. We also thank Professor Francis J. DiSalvo at Cornell University for the gift of the density measurement device. Financial support by the National Science Foundation, DMR 0313963, and by the US Department of Energy, Office of FreedomCAR and Vehicle Technologies, through the BATT program is greatly appreciated.

Supporting Information Available: Complete crystallographic, experimental, and structural data for compounds **Fe-60%** and **Fe-2/3-T** are provided in CIF format (crystallographic information file). This material is available free of charge via the Internet at http://pubs.acs.org.

CM049406R